Chemical Engineering Journal 404 (2021) 126480

Contents lists available at ScienceDirect

Chemical Engineering Journal

journal homepage: www.elsevier.com/locate/cej

A mechanistic model of direct forsterite carbonation

Andreas M. Bremen[a], Tobias Ploch[a], Adel Mhamdi[a], Alexander Mitsos[a,b,c,*]

[a] Process Systems Engineering (AVT.SVT), RWTH Aachen University, Forckenbeckstr. 51, 52074 Aachen, Germany
[b] Institute of Energy and Climate Research - Energy Systems Engineering (IEK-10), Forschungszentrum Jülich GmbH, Wilhelm-Johnen-Str., 52425 Jülich, Germany
[c] JARA-ENERGY, Templergraben 55, 52056 Aachen, Germany

HIGHLIGHTS

- A dynamic model of forsterite carbonation is presented.
- Nonideal thermodynamics of gas, liquid, and solid phases are considered.
- Discretized population balance with nucleation and growth.
- High index DAE with equilibrium and non-equilibrium reactions is reformulated.
- Evaluation of reaction conditions and future considerations in modeling carbonation.

ARTICLE INFO

Keywords:
Carbon sequestration
Mineral carbonation
Reaction kinetics
Dynamic modeling
Simulation

ABSTRACT

Mineral carbonation is a promising method to sequester large amounts of carbon dioxide and to produce value-added substitutes for the cement, paper, and plastic industries. In understanding carbonation reaction mechanisms in batch operation, dynamic models play a crucial role, and they allow to evaluate the effects of important process quantities such as temperature, pressure, particle size of solid phases and additives on reaction kinetics. We develop a mechanistic, dynamic forsterite carbonation model that accounts for gas, liquid, and multiple solid phases. In this model, gas-liquid and dissociation equilibria and surface-controlled reactions between solids and liquid phase are based on nonideal thermodynamics. We account for particle size distribution of raw material and product phases by formulating population balances considering nucleation and growth of particles. We model gas and liquid phases each as a homogeneous phase and we use isopotential conditions to describe equilibrium. The resulting high index system of differential and algebraic equations (DAE) is reformulated to obtain a DAE of differential index 1. Model predictions qualitatively match experimental data taken from literature and thus, we can quantify influences of key process conditions by simulation.

1. Introduction

In mineral carbonation processes, carbon dioxide (CO_2) can be sequestered by binding CO_2 to alkaline earth metals, e.g., to magnesium or calcium bearing minerals [1]. The reaction is spontaneous ($\Delta_r G < 0$) and the product stable. Abundant mineral deposits enable large-scale mineral carbonation for significant sequestration of anthropological carbon emissions [2,3]. Furthermore, tailor-made mineral carbonation processes may produce value-added substitutes and filling materials for the cement, plastic, and paper industries [4,5]. Therefore, this method may contribute to the reduction of the anthropological carbon footprint while supplying industry with value-added products.

Accelerated carbonation of minerals occurs by dissolving mineral feedstock and CO_2 in an aqueous solution, and precipitating mineral carbonates at increased temperature and pressure [6]. The dissociation of dissolved species, e.g., of CO_2 into bicarbonate (HCO_3^-) and carbonate (CO_3^{2-}), and interactions of the liquid phase with gas and solid phases result in a complex reactive multi-phase system. Additionally, additives such as dissociating acidic and alkaline substances strongly influence the reaction system by changing pH and dissolution/precipitation mechanisms on the surface of solid phases [7].

Experimentally, two setups have been investigated, namely direct and indirect carbonation [6]. In direct carbonation, dissolution and precipitation take place simultaneously in a single reactor [8–11]. In contrast, indirect carbonation refers to spatially-separated dissolution of feedstock material from precipitation [12,13]. The separation allows adjusting reaction conditions for each reaction step to fit the respective purpose, whereas direct carbonation benefits from lower complexity.

* Corresponding author.
E-mail address: amitsos@alum.mit.edu (A. Mitsos).

https://doi.org/10.1016/j.cej.2020.126480
Received 2 June 2020; Received in revised form 25 July 2020; Accepted 28 July 2020
Available online 04 August 2020
1385-8947/

Nomenclature

DAE	System of differential and algebraic equations
DE	Dissociation equilibrium
GLE	Gas-liquid equilibrium
HKF	Helgeson-Kirkham-Flowers
KKT	Karush-Kuhn-Tucker
NE	Non-equilibrium
ODE	Ordinary differential equation
PBE	Population balance equation
PDE	Partial differential equation
PR	Peng-Robinson
PSD	Particle size distribution
f	Final
0	Initial
C	Critical nucleus
DE	Dissociation equilibrium
eq	Equilibrium
G	Gas
GLE	Gas-liquid equilibrium
init	Initialization
L	Liquid
m	Reaction mechanism
N	Particle size node
ref	Reference
S	Solid
$\tilde{\boldsymbol{n}}$	Reformulated amount of substances vector [mol]
$\boldsymbol{x}$	Differential states [–]
α	Parameter for reinitialization of PSD [–]
$\boldsymbol{\lambda}$	Matrix of null vectors of stoichiometry matrix [–]
$\boldsymbol{\Theta}$	Parameters [–]
$\boldsymbol{y}$	Algebraic states [–]
γ	Activity coefficient [–]
ν	Stoichiometric coefficient [–]
Ω	Saturation [–]
θ	Contact angle between foreign particle and nucleus [°]
$\tilde{J}$	Thermodynamically calculated nucleation rate [1/s]
$\tilde{L}$	Size of nucleus [m]
ξ_{H^+}	Reaction order of H^+ [–]
ζ	Reaction order of solid forming ions [–]
A	Pre-exponential factor in Arrhenius term [mol/m^2/s]
a	Activity [–]
b	Molality [mol/kg]
E	Activation energy [J/mol]
f	Fugacity coefficient [bar]
G	Linear growth rate [m/s]
J	Nucleation rate [1/s]
L	Diameter of particle [m]
M	Number of species [–]
N	Number of particles [–]
n	Amount of substance [mol]
p	Pressure [bar]
r	Net reaction rate [mol/s]
S	Surface area [m^2]
T	Temperature [°C]
t	Time [s]
v^m	Molar volume [m^3/mol]

Herein, we focus on direct mineral carbonation and propose a dynamic model with the aim to examine important mechanisms and derive optimal operating conditions.

Several approaches exist to mechanistically model the interaction of aqueous systems with gas and solid phases. With high rates of gas-liquid and dissociation reactions, a common approach assumes gas and liquid species to be at chemical equilibrium. The rigorous criterion for equilibrium is global minimum of Gibbs free energy, which is challenging to implement [14–16]. Thus, isopotential is typically used to calculate the equilibrium; this is a necessary-only equilibrium criterion [17]. Even isopotential equations are sometimes difficult to solve because of different orders of magnitudes of the equilibrium, and nonlinearity due to nonideal thermodynamics. A common method is to calculate isopotential by the use of temperature-dependent equilibrium constants $K_{eq}(T)$ given in multiple databases, as applied in PHREEQC [18]. Gibbs Free Energy Minimization Software (GEMS) applies a different approach, which locally minimizes Gibbs free energy for equilibrium calculation [19]. Commercial process modeling tools such as distributed by OLI Systems [20] contain built-in thermodynamic models for complex electrolyte systems, that are used to simulate entire flowsheets with interfaces to other process engineering software such as Aspen Plus [21] and gPROMS [22]. However, to theoretically investigate mineral carbonation, which is experimentally operated in batch mode, dynamic simulation is necessary. The available commercial tools do not allow dynamic simulation with incorporation of particle size information and mole balances.

The open literature provides a limited number of mechanistic, dynamic models describing mineral carbonation. Na et al. develop a mechanistic model for the carbonation of calcium hydroxide at ambient conditions and up to a temperature of 70 °C with simplistic thermodynamic models [23]. Oliver et al. formulate a mechanistic model with focus on gas-liquid mass transfer to describe serpentinite carbonation and include thermodynamic data from PHREEQC [24]. Besides dynamic modeling, mainly calculations of phase equilibria with partial incorporation of dissolution reactions of raw material in PHREEQC and other software tools are considered [25–29]. The publication of Pan et al. gives an overview on reaction mechanisms and phenomenological modeling approaches in CO_2-mineral-water systems, but the authors do not apply them to a mineral carbonation process [30]. The recent work of Wang et al. provides a thorough experimental study of different process conditions at moderate pressures ($p < 45$ bar). They propose an empiricial correlation of mineral carbonation efficiency with different process conditions, i.e., temperature, pressure, particle size and addition of $NaHCO_3$ and NaCl [10,11]. They find a stoichiometric dissolution of feedstock particles at increased partial pressure of CO_2 and increased addition of sodium salts.

We propose a dynamic mechanistic model of direct carbonation of forsterite, that incorporates effects of pressure, temperature, additives, and particle size of solid phases including nucleation and growth. Forsterite constitutes a good substitute for widely available olivine as it contains roughly 80 mol-% of forsterite [31]. Olivine shows a similar carbonation potential as serpentine as pointed out by Ostovari et al. who investigate different reaction pathways for olivine and serpentine in a state-of-the-art scenario [32]. The choice of olivine further allows to disregard the influence of heat pretreatment, which is necessary for the use of serpentine as feedstock. In our model, we use general species mole balances that may be adapted to different mineral carbonation case studies with alternative feedstock. The model is based on detailed thermodynamics of gas, liquid and solid phases [33–39]. The model is presented in Section 2. Parameter values for incorporated thermodynamic models to describe phase interaction are taken from literature [40,37,41–44] and evaluated in Section 3. In Section 4, we demonstrate the model's applicability based on a comparison with experimental data [8,10,11] and we close with concluding remarks in Section 5.

2. Carbonation model

First, we present the model structure, which is based on the

interaction of species in different phases and introduce differential mole balance equations in Section 2.1. We set temperature T and pressure p as input to the model, thereby allowing us to omit the energy balance. The obtained model comprises a high index differential algebraic system of equations (DAE), that is analyzed and modified in Section 2.3. The DAE is nonlinear with variable values of different orders of magnitude. To alleviate this issue, we scale model equations and implement an initialization scheme discussed in Section 2.4.

2.1. Model structure and assumptions

In direct forsterite carbonation processes, solid, liquid, and gas phases are present. The raw material forsterite (Mg_2SiO_4) and gas species CO_2 dissolve in an aqueous solution and two product phases precipitate from the solution, namely magnesite ($MgCO_3$) and amorphous silica (SiO_2). Thus, the direct carbonation model consists of a gas phase (G), a liquid phase (L), and three solid phases (S) as illustrated in Fig. 1.

Gas and liquid phase are each modeled as a homogeneous phase and the solid phases are modeled as separate disperse phases as described in detail in Section 2.1.1. The reaction system encompasses dissolution of gases, liquid phase dissociations, and solid-liquid mass transfer. The gas phase containing CO_2 and H_2O is in equilibrium with the liquid phase, denoted as gas-liquid equilibrium (GLE):

$$CO_2(G) \leftrightarrow CO_2(L), \tag{1}$$

$$H_2O(G) \leftrightarrow H_2O(L). \tag{2}$$

Dissociation reactions in the liquid phase are assumed to be in equilibrium, referred to as dissociation equilibrium (DE):

$$CO_2(L) + H_2O(L) \leftrightarrow HCO_3^-(L) + H^+(L), \tag{3}$$

$$HCO_3^-(L) \leftrightarrow CO_3^{2-}(L) + H^+(L), \tag{4}$$

$$H_2O(L) \leftrightarrow OH^-(L) + H^+(L). \tag{5}$$

The equilibrium assumptions are applied to fast reactions to omit parameterization of reaction rates. Each solid phase may precipitate or dissolve depending on its saturation in the liquid phase. In mineral carbonation, rate-based surface-controlled reactions are dominating diffusive interactions between solid and liquid phases [45,46]. Wang et al. further narrowed this down to increased pressure and increased salt concentration [11].The solid-liquid mass transfer reactions are given by

$$Mg_2SiO_4(S) + 4H^+(L) \leftrightarrow 2Mg^{2+}(L) + SiO_2(L) + 2H_2O(L), \tag{6}$$

$$MgCO_3(S) \leftrightarrow Mg^{2+}(L) + CO_3^{2-}(L), \tag{7}$$

$$SiO_2(S) \leftrightarrow SiO_2(L). \tag{8}$$

Experimental observations show that an additional solid hydromagnesite ($Mg_5(CO_3)_4(OH)_2{\cdot}4H_2O$) is formed during reactor heat up at low temperature [47,30]. However, only small amounts are formed that are converted to magnesite at increased temperatures. Therefore, we neglect formation of additional phases in our model. In addition, we assume no interaction of solid phases with each other, i.e., they do not mix or coagulate. Furthermore, we do not consider breakage or agglomeration of particles. In literature on mineral carbonation, these effects have not been reported in detail at reaction conditions. Thus, kinetics, that are strongly dependent on feedstock and experimental setup, are unknown. Therefore, it is difficult to make any statement on validity of this assumption. We model nucleation effects based on classical nucleation theory [38]. According to the theory, nucleation may occur spontaneously in a solution without any solids (homogeneous nucleation), by formation on dissimilar solid particles (heterogeneous nucleation), or from attrition of solid particles, e.g., due to stirring or collision of particles (secondary nucleation) [38]. Homogeneous nucleation takes place only in the absence of foreign particles and secondary nucleation rates are orders of magnitudes lower at increased saturation compared to heterogeneous nucleation rates, e.g., shown for the case of gypsum nucleation [48]. Therefore, we assume only heterogeneous nucleation on undissolved forsterite particles as the nucleation mechanism.

We formulate general mole balances for M_G gaseous and M_L liquid species as follows:

$$\dot{n}_{G,i}(t) = \sum_{j=1}^{M_{GLE}} \nu_{G,i,j}^{GLE} r_j^{GLE}(t), \quad i = 1, \ldots, M_G, \tag{9}$$

$$\dot{n}_{L,i}(t) = r_{L,i}^{s}(t) + \sum_{j=1}^{M_{GLE}} \nu_{L,i,j}^{GLE} r_j^{GLE}(t) + \sum_{j=1}^{M_{DE}} \nu_{L,i,j}^{DE} r_j^{DE}(t), \quad i = 1, \ldots, M_L, \tag{10}$$

$$n_{G,i}(t=0) = n_{G,i}^0, \quad i = 1, \ldots, M_G, \tag{11}$$

$$n_{L,i}(t=0) = n_{L,i}^0, \quad i = 1, \ldots, M_L, \tag{12}$$

where $n_{G,i}$ and $n_{L,i}$ are the amounts of substance of species i in the gas and liquid phase, respectively, and M_{GLE} and M_{DE} are the number of GLE and DE reactions. $\nu_{G,i,j}^{GLE}$, $\nu_{L,i,j}^{GLE}$, and $\nu_{L,i,j}^{DE}$ are stoichiometric coefficients and r_j^{GLE} and r_j^{DE} denote the GLE and DE net reaction transfer rates, respectively. Note that mass transfer between phases is considered as a reaction here. Due to the equilibrium assumptions, no explicit algebraic equations are given for r_j^{GLE} and r_j^{DE}, cf. Section 2.3. $r_{L,i}^{s}$ denotes the overall mass transfer rate from solid phases into the liquid phase given in the following section.

2.1.1. Modeling of solid phases

We model each solid phase as a pure disperse phase formulated as a population balance equation (PBE). That way, we account for the surface area and particle size distribution (PSD) of the solid phases.

The general population balance equation for a solid phase k reads

$$\left.\frac{\partial N_{S,k}}{\partial t}\right|_{t,L_{S,k}} + \left.\frac{\partial (G_{S,k} \cdot N_{S,k})}{\partial L_{S,k}}\right|_{t,L_{S,k}} = J_{S,k}\left(t, L_{S,k}\right), \quad k = 1, \ldots, M_S, \tag{13}$$

where $N_{S,k}$ is the number of particles in diameter range $(L_{S,k}, L_{S,k} + \mathrm{d}L_{S,k})$, $G_{S,k}$ is the radial growth rate of particle with diameter $L_{S,k}$, and $J_{S,k}$ is the nucleation rate of particle size $L_{S,k}$.

Mantzaris et al. provide robust and computationally efficient

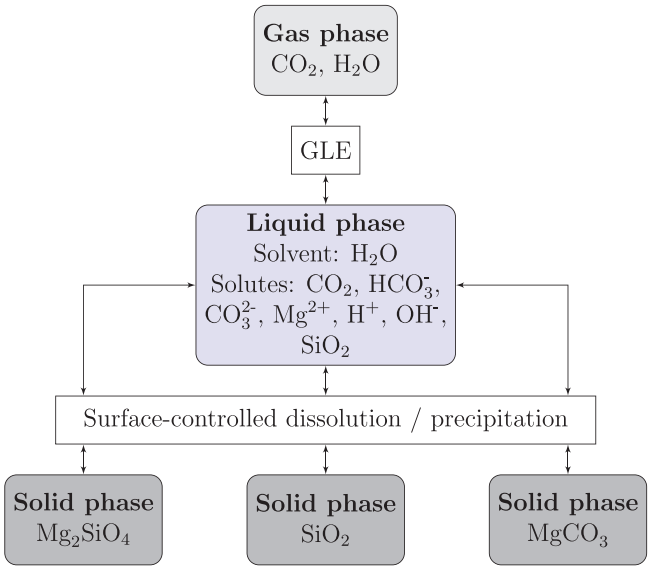

Fig. 1. Structure of carbonation model with one homogeneous gas phase, one homogeneous liquid phase, three disperse solid phases (each contains a single species), and their interactions.

methods to numerically solve partial differential equations (PDE) arising from population balance equations. They convert the PDE to ordinary differential equations (ODE) based on finite difference methods [49], spectral methods [50] and finite volume methods [51] and provide numerically stable integration algorithms. Since our focus is to model the mineral carbonation system as DAE, we transform the PDE in Eq. (13) into a system of ordinary differential equations (ODE). An intuitive approach is to discretize the partial derivative with respect to particle size $L_{S,k}$, e.g., by a finite-difference discretization for simultaneous growth and nucleation [52]. However, a high number of nodes is needed to keep numerical diffusion low. Instead, we use the *method of characteristics* to solve the PBE [53]. Rather than defining a constant grid of particle sizes, the particle size $L_{S,k,l}$ changes with the growth rate $G_{S,k,l}$ of solid phase k at particle size node l. Assuming constant molar volume $v_{S,k}^{m,\mathrm{ref}}$ of solid k, Eq. (13) can be reformulated to

$$\dot{L}_{S,k,l}(t) = G_{S,k,l}(t), \quad k = 1, \ldots, M_S,\ l = 1, \ldots, M_N, \tag{14}$$

$$L_{S,k,l}(t=0) = L_{S,k,l}^0, \quad k = 1, \ldots, M_S,\ l = 1, \ldots, M_N, \tag{15}$$

where $L_{S,k,l}$ is the particle size of solid phase k at particle size node l, M_N is the total number of particle nodes, and $L_{S,k,l}^0$ is the initial particle size.

The change in molar volume at varying temperature and pressure calculated from the equation of state [54] is low and therefore, the assumption of constant molar volume $v_{S,k}^{m,\mathrm{ref}}$ of solid phase k is justified. Assuming spherical particles, the linear growth rate is given by

$$G_{S,k,l} = -2 r_{S,k,l} v_{S,k}^{m,\mathrm{ref}}, \quad k = 1, \ldots, M_S,\ l = 1, \ldots, M_N, \tag{16}$$

where $r_{S,k,l}$ is the solid-liquid mass transfer rate of one particle at size node l. Note that $r_{S,k,l}$ is greater than zero for dissolution and less than zero for precipitation. The mole amount of one particle at size node l is then calculated by

$$n_{S,k,l} = \frac{\pi}{6} \frac{(L_{S,k,l})^3}{v_{S,k}^{m,\mathrm{ref}}}, \quad k = 1, \ldots, M_S,\ l = 1, \ldots, M_N. \tag{17}$$

Eq. (14) only discloses the particle size of each node. Therefore, we need additional differential equations to consider the number of particles $N_{S,k,l}$ of solid phase k at particle size node l:

$$\dot{N}_{S,k,l}(t) = J_{S,k,l}(t), \quad k = 1, \ldots, M_S,\ l = 1, \ldots, M_N, \tag{18}$$

$$N_{S,k,l}(t=0) = N_{S,k,l}^0, \quad k = 1, \ldots, M_S,\ l = 1, \ldots, M_N, \tag{19}$$

where $J_{S,k,l}$ and $N_{S,k,l}^0$ are the nucleation rate and initial number of particles of solid species k at particle size node l, respectively. Particles with critical nucleation size $\widetilde{L}_{S,k}$ nucleate only in the next larger particle size node $L_{S,k,C}$, as illustrated in Fig. 2. Thus, the nucleation rate $J_{S,k,l}$ is given by

$$J_{S,k,l} = \begin{cases} \widetilde{J}_{S,k}, & \text{if} L_{S,k,l-1} < \widetilde{L}_{S,k} \leqslant L_{S,k,l}, \\ 0, & \text{otherwise}, \end{cases} \quad k = 1, \ldots, M_S,\ l = 1, \ldots, M_N, \tag{20}$$

where $\widetilde{J}_{S,k}$ is the thermodynamically calculated nucleation rate from classical nucleation theory [38]. Note that in heterogeneous nucleation, the contact angle $\Omega_{S,k}$ between foreign particle and precipitating particle is decisive for nucleation and thus evaluated in detail in Section 4.1.

Since the growth of particle nodes $L_{S,k,l}$ is greater than $\widetilde{L}_{S,k,C}$ and non-constant $\widetilde{L}_{S,k,C}$, the particle node $L_{S,k,C}$ – where nucleation takes place – may diverge from the thermodynamically calculated nucleation particle size $\widetilde{L}_{S,k,C}$ [38]. To ensure that $L_{S,k,C}$ is always in the range of $\widetilde{L}_{S,k,C}$, a new node of size $\widetilde{L}_{S,k,C}$ and initial zero particle number is added to the differential states when the condition

$$L_{S,k,C} \leqslant \alpha_{S,k} \widetilde{L}_{S,k,C}, \ k = 1, \ldots, M_S \tag{21}$$

is violated. The parameter $\alpha_{S,k}$ is greater than 1. Nucleation kinetics become more accurate, the closer $\alpha_{S,k}$ tends to 1 due to increased addition of new nodes. However, at the same time, the number of differential equations increases. Therefore, we set the parameter value to $\alpha_{S,k} = 1.03$, which results in a fine grid in the range of nucleating particle size and a coarse grid for growing particles.

The surface-controlled dissolution rate for solid phase k at particle size node l reads [39]

$$r_{S,k,l} = S_{S,k,l} \sum_{j=1}^{M_{m,k}} \left[A_{S,k,j} \exp\left(-\frac{E_{S,k,j}}{RT}\right) a_{H^+}^{\xi_{H^+,S,k,j}} (1 - \Omega_{S,k,l})^{\zeta_{S,k,j}} \right], \quad k = 1, \ldots, M_S,\ l = 1, \ldots, M_N. \tag{22}$$

where $S_{S,k,l}$ and $\Omega_{S,k,l}$ are the surface area and saturation in the liquid phase of solid phase k with particle size l. $M_{m,k}$ is the number of reaction mechanisms of solid phase k. $A_{S,k,j}$ and $E_{S,k,j}$ are pre-exponential factor and the activation energy in the corresponding Arrhenius term. a_{H^+} and $\xi_{H^+,S,k,j}$ are the activity of H^+ and its reaction order, and $\zeta_{S,k,j}$ is the reaction order with respect to solid forming ions. We use rate parameter values given in a compilation for numerous minerals [43].

With the phenomena of growth and nucleation, the overall mass transfer from solid phases to species i in the liquid phase denoted as $r_{L,i}^s$ in Eq. (10) is given as

$$r_{L,i}^s = \sum_{k=1}^{M_S} \nu_{S,k,i} \left[\sum_{l=1}^{M_N} N_{S,k,l} r_{S,k,l} - \frac{\pi}{6} \frac{(L_{S,k,C})^3}{v_{S,k}^{m,\mathrm{ref}}} \widetilde{J}_{S,k} \right], \quad i = 1, \ldots, M_L, \tag{23}$$

where the first term in the brackets accounts for growth of each particle size node l and the second term accounts for nucleation of solid species k. $\nu_{S,k,i}$ is the stoichiometric coefficient of solute i forming solid phase k.

2.2. Thermodynamic models

Carbonation of forsterite is experimentally reported to have favorable operating conditions at a pressure up to 150 bar and a temperature of 185 °C [8,9]. The proposed model uses detailed thermodynamics in this range for calculation of saturation of solid phases, isopotential of DE and GLE, and calculation of phase volumes.

Solute properties at infinite dilution are based on the revised Hegeson-Kirkham-Flowers (HKF) equation of state [34] with parameter values taken from the software package SUPCRTBL [40]. In contrast to [40], water (solvent) properties are calculated with the temperature and pressure explicit Helmholtz model IF97 [36] instead of IAPWS84 [55]. In general, solvent property models used for parameterization of the HKF model should be applied when using these parameter values. However, discrepancies at temperatures below 500 °C are small when using different solvent property models [56]. To account for nonideal contribution at increased ionic strength, the Bromley equation with Meissner extension for increased temperature is applied [41,42]. When applying this method in modeling mineral carbonation, a major drawback emerges, as temperatures up to 200 °C are possible, exceeding the temperature limit of 150 °C given in [42]. Since alternative parameterized models to determine activity coefficients in mixed electrolyte systems at increased ionic strength and temperature are not available, we stick to the Bromley model with Meissner extension as excess Gibbs free energy model for solutes. We consider the volume contribution of

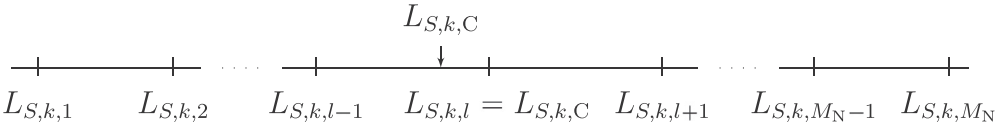

Fig. 2. Particle nucleation on particle size grid with $\widetilde{L}_{S,k,C}$ being the critical nucleation size.

solutes to overall volume of the liquid phase to be ideal.

We assume pure solid phases that do not intermix with each other and activities are therefore always unity. We adapt the heat capacity polynomial and the equation of state for solids [54] with parameters from SUPCRTBL for calculation of chemical potential of solids and assume constant molar volume $v_k^{m,\mathrm{ref}}$. Present solid phases in our model do not undergo phase transition which is therefore excluded in our model.

Gas volume is calculated from Peng-Robinson (PR) equation of state [37] with parameters from [44]. The PR model in combination with a heat capacity polynomial from SUPCRTBL accounts for calculation of Gibbs free energy at temperature and pressure of interest.

2.3. DAE analysis

The proposed discretized model with temperature T and pressure p as inputs is a semi-explicit DAE:

$$\dot{\boldsymbol{x}}(t) = \boldsymbol{f}(\boldsymbol{x}(t), \boldsymbol{y}(t), \boldsymbol{u}(t), \boldsymbol{\Theta}), \tag{24}$$

$$\boldsymbol{0} = \boldsymbol{g}(\boldsymbol{x}(t), \boldsymbol{y}(t), \boldsymbol{u}(t)) \tag{25}$$

where $\boldsymbol{x}(t)$ and $\boldsymbol{y}(t)$ are the differential and algebraic states, respectively, $\boldsymbol{\Theta}$ are parameters, and $\boldsymbol{u}(t)$ the inputs to the differential and algebraic equations $\boldsymbol{f}$ and $\boldsymbol{g}$, respectively. Common numerical solvers can solve DAE systems of differential index 1 [57]. In the proposed model, the algebraic states r_j^{DE} and r_j^{GLE} denoting net reaction rates of DE and GLE, respectively, only appear in differential Eqs. (9) and (10), but not in algebraic equations. The only implicit information with respect to these rates is given by isopotential conditions. Consequently, the algebraic equations cannot be solved for r_j^{DE} and r_j^{GLE} and thus, the differential index is higher than 1 [58]. Originally, the same formulation of reaction systems with equilibrium assumptions is obtained by a time-scale analysis of a dynamic reaction system with fast and slow reactions [59–61]. In the time-scale of slow reactions, the differential equations may be transformed into a DAE of high index by a singular perturbation, where the obtained algebraic equations then denote the isopotential condition. Common methods to reduce the differential index of the DAE system to 1 are differentiation [62] and reformulation [63]. The differentiation of algebraic equations avoids loss of information on reaction rates r_j^{DE} and r_j^{GLE}, but is cumbersome to realize due to the nonlinearity of the system. We thus follow the reformulation method proposed in [63], and reformulate the DAE by eliminating r_j^{DE} and r_j^{GLE} from the DAE. The model complexity remains similar to the original model [63]. For the reformulation, we collect all gas and liquid species moles in a vector $\boldsymbol{n} \in \mathscr{R}^{M_{\mathrm{L}}+M_{\mathrm{G}}}$ and combine the species mole balances given in Eqs. (9) and (10) as:

$$\dot{\boldsymbol{n}}(t) = \boldsymbol{r}^s(t) + \boldsymbol{\nu}^{\intercal}\boldsymbol{r}(t), \tag{26}$$

where $\boldsymbol{r}^s$ comprises solid-liquid mass transfer rates, which are zero for gas species. The vector $\boldsymbol{r}(t) \in \mathscr{R}^{M_{\mathrm{DE}}+M_{\mathrm{GLE}}}$ contains GLE and DE reaction rates, and $\boldsymbol{\nu} \in \mathscr{R}^{(M_{\mathrm{DE}}+M_{\mathrm{GLE}})\times(M_{\mathrm{L}}+M_{\mathrm{G}})}$ is the corresponding stoichiometric matrix. From a Gauss-Jordan algorithm, we calculate a matrix $\boldsymbol{\lambda} \in \mathscr{R}^{(M_{\mathrm{L}}+M_{\mathrm{G}})\times(M_{\mathrm{L}}+M_{\mathrm{G}}-M_{\mathrm{DE}}-M_{\mathrm{GLE}})}$ for which

$$\boldsymbol{\lambda}^{\intercal}\boldsymbol{\nu}^{\intercal} = \boldsymbol{0} \tag{27}$$

holds, i.e., $\boldsymbol{\lambda}$ is the nullspace of stoichiometry matrix $\boldsymbol{\nu}$. We multiply Eq. (26) by $\boldsymbol{\lambda}^{\intercal}$ to obtain

$$\boldsymbol{\lambda}^{\intercal}\dot{\boldsymbol{n}}(t) = \boldsymbol{\lambda}^{\intercal}\boldsymbol{r}^s(t) + \boldsymbol{\lambda}^{\intercal}\boldsymbol{\nu}^{\intercal}\boldsymbol{r}(t), \tag{28}$$

or equivalently

$$\dot{\tilde{\boldsymbol{n}}}(t) = \boldsymbol{\lambda}^{\intercal}\boldsymbol{r}^s(t) \tag{29}$$

with initial conditions

$$\tilde{\boldsymbol{n}}(t=0) = \boldsymbol{\lambda}^{\intercal}\boldsymbol{n}^{\mathrm{NE},0}, \tag{30}$$

where $\tilde{\boldsymbol{n}} = \boldsymbol{\lambda}^{\intercal}\boldsymbol{n}$. $\boldsymbol{n}^{\mathrm{NE},0}$ is a vector of initial gas and liquid species moles not in equilibrium (NE) further discussed in the following section. We replace species mole balances given in Eqs. (9) and (10) with Eq. (29) and obtain a reduced number of differential states $\tilde{\boldsymbol{n}}(t) \in \mathscr{R}^{(M_{\mathrm{L}}+M_{\mathrm{G}}-M_{\mathrm{DE}}-M_{\mathrm{GLE}})}$. This reformulation eliminates r_j^{DE} and r_j^{GLE} and thus, we obtain a DAE of differential index 1.

2.4. DAE initialization

The index-reduced mineral carbonation model of differential index 1 consists of $(M_{\mathrm{L}} + M_{\mathrm{G}} - M_{\mathrm{DE}} - M_{\mathrm{GLE}} + 2M_{\mathrm{S}}M_{\mathrm{N}})$ differential equations given in Eqs. (14), (18) and (29). Therefore, the same number of initial conditions has to be provided. By providing both the initial particle sizes $L_{\mathrm{S},k,l}(t=0)$ and the initial numbers $N_{\mathrm{S},k,l}(t=0)$ of each solid phase k and particle size node l, the solid phases are fully initialized. These initial conditions can be determined by PSD measurements. For precipitating phases that are initially not present, $L_{\mathrm{S},k,l}(t=0)$ and $N_{\mathrm{S},k,l}(t=0)$ are set to zero. Finally, initial conditions for differential states $\tilde{\boldsymbol{n}}$ are determined. For this purpose, similar to the reformulation of gas and liquid species mole balances in the previous section, the set of initial conditions is given in Eq. (30). Here, $\boldsymbol{n}^{\mathrm{NE},0}$ consists of gas and liquid species moles added to the system before equilibration [63]. We therefore determine initial amounts of each species $\boldsymbol{n}^{\mathrm{NE},0}$ to calculate $\tilde{\boldsymbol{n}}(t=0)$. The initial state of the DAE is at DE and GLE and therefore $n_{\mathrm{G},i}(t=0) \neq n_{\mathrm{G},i}^{\mathrm{NE},0}$ and $n_{\mathrm{L},i}(t=0) \neq n_{\mathrm{L},i}^{\mathrm{NE},0}$. By providing the initial conditions for solid phases $L_{\mathrm{S},k,l}(t=0)$, and $N_{\mathrm{S},k,l}(t=0)$ and initial values for $\tilde{\boldsymbol{n}}(t=0)$, the model is fully initialized. The determination of the initial amounts of gas and liquid species $n_{\mathrm{G},i}^{\mathrm{NE},0}$ and $n_{\mathrm{L},i}^{\mathrm{NE},0}$ is, however, not always trivial in case of overall volume and initial pressure requirements of the system, i.e., if the overall volume is fixed and not all mole quantities can be freely chosen. For this purpose, an implicit system of algebraic equations must be solved in order to obtain initial moles $n_{\mathrm{G},i}^{\mathrm{NE},0}$ and $n_{\mathrm{L},i}^{\mathrm{NE},0}$, and thus $\tilde{\boldsymbol{n}}(t=0)$. Without good initial guesses, the implicit system of algebraic equations is difficult to solve due to different orders of magnitudes of variable values. Therefore, we alternatively use a dynamic initialization model proposed by Zinser et al. to calculate chemical and phase equilibria and to obtain initial values $\tilde{\boldsymbol{n}}(t=0)$ while considering volume and pressure constraints [64]. The general idea is to write dynamic mole balances without isopotential conditions, but instead defining net reaction rates $r_j^{\mathrm{GLE,init}}$ and $r_j^{\mathrm{DE,init}}$ that tend towards equilibrium. In our case, we write dynamic mole balances of gas and liquid species as in Eqs. (9) and (10), but without mass transfer from non-equilibrium solid phases:

$$\dot{n}_{\mathrm{G},i}(t) = \sum_{j=1}^{M_{\mathrm{GLE}}} \nu_{\mathrm{G},i,j}^{\mathrm{GLE}} r_j^{\mathrm{GLE,init}}(t), \quad i = 1, \ldots, M_{\mathrm{G}}, \tag{31}$$

$$\dot{n}_{\mathrm{L},i}(t) = \sum_{j=1}^{M_{\mathrm{GLE}}} \nu_{\mathrm{L},i,j}^{\mathrm{GLE}} r_j^{\mathrm{GLE,init}}(t) + \sum_{j=1}^{M_{\mathrm{DE}}} \nu_{\mathrm{L},i,j}^{\mathrm{DE}} r_j^{\mathrm{DE,init}}(t), \quad i = 1, \ldots, M_{\mathrm{L}}. \tag{32}$$

Net reaction rates $r_{i,j}^{\mathrm{GLE,init}}$ and $r_{i,j}^{\mathrm{DE,init}}$ are defined as the distance between non-equilibrium and equilibrium state being the driving force [64]:

$$r_j^{\mathrm{GLE,init}} = k_j^{\mathrm{GLE,init}} \left(K_j^{\mathrm{GLE}} - \prod_{i=1}^{M_{\mathrm{G}}} \left(\frac{f_i}{p^{\mathrm{ref}}} \right)^{\nu_{\mathrm{G},i,j}^{\mathrm{GLE}}} \cdot \prod_{i=1}^{M_{\mathrm{L}}} a_i^{\nu_{\mathrm{L},i,j}^{\mathrm{GLE}}} \right), \quad j = 1, \ldots, M_{\mathrm{GLE}}, \tag{33}$$

$$r_j^{\mathrm{DE,init}} = k_j^{\mathrm{DE,init}} \left(K_j^{\mathrm{DE}} - \prod_{i=1}^{M_{\mathrm{L}}} a_i^{\nu_{\mathrm{L},i,j}^{\mathrm{DE}}} \right), \quad j = 1, \ldots, M_{\mathrm{DE}}, \tag{34}$$

where $k_j^{\mathrm{GLE,init}}$ and $k_j^{\mathrm{DE,init}}$ are parameters without physical meaning, K_j^{DE} and K_j^{GLE} are equilibrium constants, f_i is the fugacity coefficient of gas species i and a_i is the activity of liquid species i. By providing $M_{\mathrm{L}} + M_{\mathrm{G}}$ initial conditions, e.g., $M_{\mathrm{L}} + M_{\mathrm{G}} - 1$ species moles and an overall volume V, the DAE is fully initialized and can be solved for a time frame t_f until steady state, i.e., $r_j^{\mathrm{GLE,init}} \to 0$ and $r_j^{\mathrm{DE,init}} \to 0$. Then,

with final states $n_{G,i}(t_f)$ and $n_{L,i}(t_f)$, the initial conditions $\tilde{\boldsymbol{n}}(t=0)$ can be calculated from Eq. (30). Furthermore, final values of algebraic states are used as initial guesses for efficient initialization of the DAE at GLE and DE. Specifically, we use final values of the initialization simulation to give initial guesses for mole fractions y_i and x_i in gas and liquid phase, respectively, activity coefficients γ_i, and molar volume of the gas phase v^g.

3. Applicability of thermodynamic models

Since thermodynamic property models and parameters are taken from various sources, we compare thermodynamic models given in Section 2.2 with experimental results at different temperatures, pressures, and ionic strengths. Fig. 3 illustrates simulation results of a liquid phase containing NaCl in equilibrium with a gas phase consisting of CO_2 and H_2O. The comparison of our results with experimental data [65] and a model based on regression of experimental data [66] shows that our proposed model generally underestimates the dissolution of CO_2 in water with increasing differences at high pressure. With increasing molality of NaCl, the differences are reduced. The referenced model (green lines in Fig. 3) uses two different models for different temperature regimes and does not consider dissociation of species [66]. Furthermore, they carry out a regression in each temperature regime to match an experimental data compilation. For the consideration of the system of $H_2O - CO_2 - NaCl$, the referenced model [66] shows accurate predictions. In our proposed model, each phase is based on one nonideal thermodynamic model with parameter values taken from different references. The discrepancies at increased pressures arise because only ionic strength dependent activity coefficient of neutral species are taken into account to describe the salting out effect ($\ln\gamma_{CO_2} = bI$, where b is a constant). The activity model is missing consideration of interaction of alike neutral species and of neutral species with water. At the same time, the choice of thermodynamic models allows to take CO_2 dissociation reactions into account. Due to low dissociation of CO_2 in water, dissociated species HCO_3^-, CO_3^{2-}, OH^-, and H^+ are not plotted in Fig. 3. Considering dissociation reactions enables the model to calculate pH in the solution, which is an essential factor for mineral carbonation. Experimental data [67] shows that the pH is predicted within the confidence interval of experiments at temperatures up to $T = 100$ °C. Experimental data on pH for temperatures $T > 100$ °C are not available and therefore the pH in Fig. 3b cannot be evaluated. With the implemented thermodynamics, increased NaCl molality has minor influence on pH at $T = 200$ °C. In the following, the evaluated thermodynamic models serve as a basis for simulation of our mineral carbonation model.

4. Insights from carbonation model simulation

The presented model is implemented in Modelica [68] and simulated using Dymola 2020 [69]. The implemented model including presented simulation results is provided in the Supplementary Information. We use the DAE integrator DASSL [70] with an integration tolerance 10^{-8}. Since the number of states in the equation-oriented modeling language Modelica has to be constant during simulation, we introduce dummy differential states $L_{S,k,l}$ and $N_{S,k,l}$ that are initially zero and are reinitialized, whenever the condition in Eq. (21) is violated. Our proposed model has several degrees of freedom, namely temperature, pressure, initial PSD, amount of feedstock forsterite, and initial amount of H_2O, CO_2 and additives. Furthermore, unknown parameter values exist, i.e, contact angles between feedstock and precipitating phases $\theta_{S,MgCO_3}$ and θ_{S,SiO_2}. Since detailed kinetics of nucleation of product phases on feedstock particles are not given in literature, we first perform a sensitivity study with respect to unknown contact angles $\theta_{S,MgCO_3}$ and θ_{S,SiO_2} in Section 4.1. Subsequently, we investigate the influence of remaining degrees of freedom on model predictions for fixed contact angles in Section 4.2.

4.1. Influence of unknown contact angles at varying temperature and pressure

To investigate the influence of unknown contact angles $\theta_{S,MgCO_3}$ and θ_{S,SiO_2} on carbonation, we compare the model predictions for varying parameter values to experimental data from literature. For this purpose, we set contact angles to the equal value $\theta = \theta_{S,MgCO_3} = \theta_{S,SiO_2}$ and use experimental data from a compilation of numerous fed-batch carbonation experiments at constant temperature and pressure [8]. The experimental data is obtained at mixtures of $0.64 mol_{NaHCO_3}/kg_{solvent}$ and $1 mol_{NaCl}/kg_{solvent}$ in the liquid phase and the authors find that this composition cuts experimental time by a factor of four while obtaining similar yields. In a first step, to disregard the effect of additives, we set the simulation horizon to four times the experimental time ($t_f = 4$ h) and analyze influence of additives afterwards. We set the initial amount of solids in the system to 15 wt.% as reported in the experiments. However, instead of providing detailed PSD of feedstock, O'Connor et al. only state feedstock particles to be <75 μm. In order to investigate the sensitivity of contact angles $\theta_{S,k}$ of precipitating species $MgCO_3$ and SiO_2, we set the initial PSD of feedstock to a mean value of $L_{Mg_2SiO_4} = 30$ μm with standard deviation $\sigma = 5$ μm.

Fig. 4a illustrates the influence of pressure on the extent of carbonation at constant temperature $T = 185$ °C. The experimental data shows an increased extent of reaction for high pressures. This trend is also reflected in the simulation results for all contact angles resulting from increased molality of CO_2. Fig. 4b shows the temperature dependence on extent of carbonation. We do not show simulation results for temperatures below 150 °C since the model does not account for

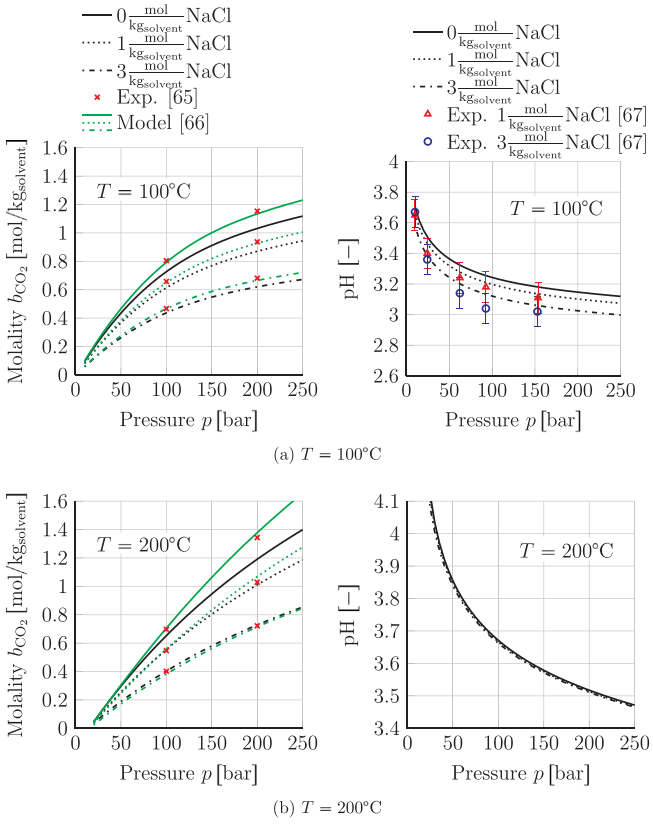

Fig. 3. Molality of CO_2 and pH over pressure p in different NaCl solutions at (a) 100 °C and (b) 200 °C. We compare our model (black lines) with a model by [66] (green lines), experimental data of m_{CO_2} with uncertainty of ± 0.57% [65] and experimental data of pH at $1\frac{mol}{kg_{solvent}}$ and $3\frac{mol}{kg_{solvent}}$ NaCl with uncertainty of ± 0.2 pH units at 95% confidence [67]. No experimental data is available on pH at $T = 200$ °C. (For interpretation of the references to colour in this figure legend, the reader is referred to the web version of this article.)

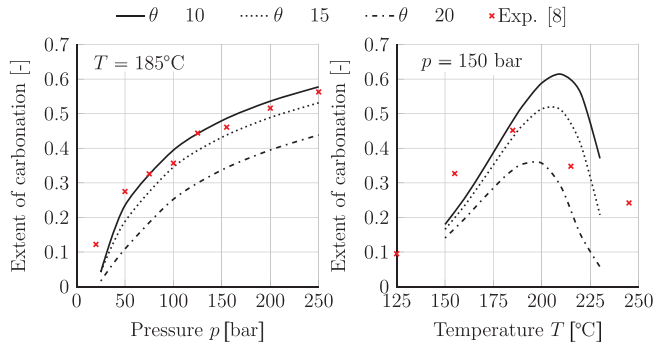

(a) Extent of carbonation for different contact angles over pressure compared with experimental data [8].

(b) Extent of carbonation for different contact angles over temperature compared with experimental data [8].

Fig. 4. Influence of contact angle $\theta_{S,MgCO_3}$ and θ_{S,SiO_2} set to the same value on extent of carbonation of solids after simulation horizon of $t_f = 4$ h compared to experimental data [8]: (a) Extent of carbonation increases with increasing pressure and reduced contact angle; (b) Extent of carbonation shows a maximum for each contact angle qualitatively similar to experimental data.

formation of hydrated magnesium carbonates that are observed experimentally at lower temperatures. Temperature influence shows a maximum in experiments at 185 °C at 150 bar. Simulation results for different contact angles qualitatively show a maximum, as well. However, for chosen PSD the maximum is at higher temperatures. Most recently, a compilation on different experimental data from different references shows an optimal temperature range for olivine carbonation of 185–200 °C [71]. Wang et al. find a maximum at $T = 175$ °C for their experimental investigation of temperature influence at moderate pressure ($p < 45$ bar) [10,11]. Simulations at the same reaction conditions with particle size between 0 and 25 μm without consideration of additives and a simulation horizon of $t^f = 5$ h similarly show a maximum at lower temperature of $T \approx 170$ °C, illustrated in Fig. 5b. The lower temperature optimum may result from a reduced concentration of carbon species due to lower pressure. The pressure influence shown in Fig. 5a shows a similar trend as in Wang et al., however with lower overall conversions. In general, our model underestimates conversions achieved by Wang et al.

In summary, temperature and pressure influence seem to be sufficiently consistent with the experimental data for contact angles of $\theta_{S,MgCO_3} = 15°$ and $\theta_{S,SiO_2} = 15°$. If we take into account different experimental data with focus on product particle size [72,73], magnesite particles and amorphous silica particles are obtained in the particle size order of μm and nm, respectively. The model predicts product particle sizes in the same order of magnitude.

4.2. Model predictions of influence of relevant inputs

For the analysis of relevant model inputs, we use fixed contact angles of $\theta_{S,MgCO_3} = 15°$ and $\theta_{S,SiO_2} = 15°$. We now consider the influence on carbonation of the model inputs PSD, and additives, as temperature and pressure influence is readily investigated in the previous section.

4.2.1. Influence of particle size

In mineral carbonation, the particle size of raw material and its particle size distribution are important factors for carbonation. In general, a feed of large feedstock particles is desirable due to the high energy demand for grinding. However, the specific surface area correlates quadratically to particle size, and, therefore, dissolution rate given in Eq. (22) is drastically reduced. The trade-off between energy demand and dissolution rate is not part of this study, but we can quantify the influence of particle size on carbonation. Fig. 6 shows the amount of magnesite obtained for different initial mean particle sizes of forsterite.

We compare the original case with initial particle size distribution with mean particle size $L_{Mg_2SiO_4} = 30$ μm and standard deviation $\sigma = 5$ μm with two other cases with mean particle sizes of $L_{Mg_2SiO_4} = 10$ μm and $L_{Mg_2SiO_4} = 60$ μm and standard deviations of $\sigma = 2$ μm and $\sigma = 5$ μm, respectively. The simulations in all three cases show that within the first minutes, particles nucleate to create sufficient surface area for their subsequent growth. The remaining simulation horizon is dominated by growth of nucleated particles. The growth of magnesite particles is faster for higher surface area of forsterite resulting in higher amounts of product. Consequently, the reduction of forsterite particle size shows a positive and strong effect on carbonation. By reducing mean particle size from $L_{Mg_2SiO_4} = 60$ μm to $L_{Mg_2SiO_4} = 10$ μm the extent of carbonation can be increased from about 40% to almost 100% within a simulation horizon of 6 h.

O'Connor et al. [8] report experiments on carbonation of synthetic forsterite with a retention time of 3 h and they obtain 76% extent of carbonation for particle sizes smaller 45 μm at 186 °C and pressure ranging from 126 to 107 bar. With the assumption of small initial PSD ($L_{Mg_2SiO_4} = 10$ μm, $\sigma = 2$ μm), the simulation results are in the range of their experimental data after a simulation horizon of 3 h. Wang et al. show a strong influence of feedstock particle size, i.e., a strong increase of amount of carbonates with reduced particle size [10,11]. They provide data for specific surface area of feedstock particles, namely $1.53 m^2/g$ for feedstock particles in the range of $0 - 25$ μm. The simulation scenarios from Fig. 5 with an initial particle size of $0 - 25$ μm yield a specific surface area of $0.50 m^2/g$ due to the assumption of spherical particles. Therefore, shape factors for rigorous representation of specific surface area seem to be necessary to quantitatively predict influence of particle size. In summary, the model qualitatively matches experimental data and thus may form the basis for quantification of the trade-off between particle size and grinding energy.

4.2.2. Influence of additives

In literature, two assumptions of the mechanistic effect of additives are found. First of all, additives may accelerate feedstock dissolution by effects on the surface of feedstock material, i.e., by influencing the surface charge [8]. Secondly, additives may buffer the liquid phase to a pH that is beneficial for mineral carbonation, i.e., by providing sufficient dissociated CO_2 [28]. Various bicarbonate salts ($NaHCO_3$, $KHCO_3$, and $RbHCO_3$) with the same molalities and complete dissociation show different effects on carbonation [74]. Therefore, not only the buffered solution, but also positively charged ions Na^+, K^+ and Rb^+ have enhancing effects on the surface of feedstock material. Wang et al. find that the formation of a passivating layer limiting further dissolution is prevented by addition of $NaHCO_3$, which supports the surface enhancing effects of bicarbonates [11]. It has also been reported that organic acids, e.g. oxalic acid, have a positive effect on mineral carbonation by

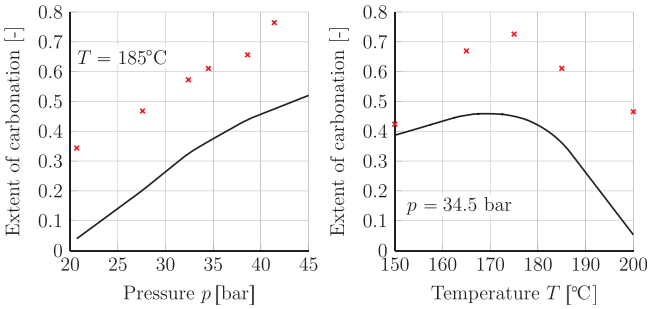

(a) Extent of carbonation over pressure compared with experimental data [11].

(b) Extent of carbonation over temperature compared with experimental data [11].

Fig. 5. Comparison of simulation results with experimental data [11]. Simulations are carried out with simulation horizon of $t^f = 5$h, initial PSD of feedstock between 0 and 25 μm taken from [11] and without consideration of additives. Comparison shows qualitative agreement of temperature and pressure influence.

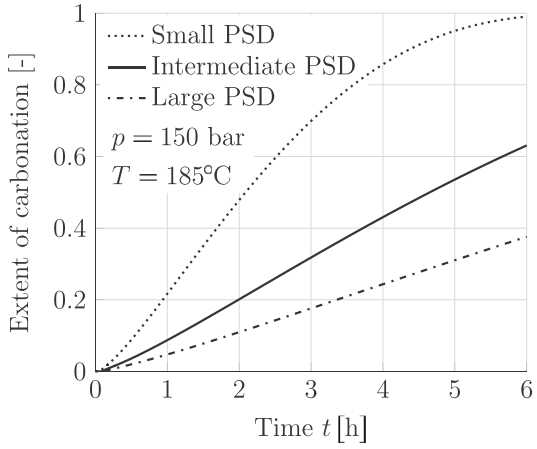

Fig. 6. Influence of initial forsterite particle size on extent of carbonation with simulation horizon of 6 h at 150 bar and 185 °C. Large, intermediate and small initial particle sizes with mean at $L_{Mg_2SiO_4} = 60$ μm, $L_{Mg_2SiO_4} = 30$ μm and $L_{Mg_2SiO_4} = 10$ μm and standard deviation $\sigma = 5$ μm, $\sigma = 5$ μm, $\sigma = 2$ μm, respectively.

leaching Mg^{2+} ions on the surface of feedstock particles [75,12]. However, organic acids may thermally decompose at temperatures necessary for carbonation [76], and thus, their use should be avoided.

With the proposed model, only the buffering effects of additives can be evaluated. We compare a simulation with and without the use of $0.64 mol_{NaHCO_3}/kg_{solvent}$ and $1 mol_{NaCl}/kg_{solvent}$ while keeping all other model inputs fixed. With initial 15 wt.% feedstock, simulation horizon of 4 h, mean particle size of 30 μm with standard deviation of 5 μm and constant temperature and pressure of 185 °C and 150bar, respectively, the investigation indicates (results not shown) an extent of carbonation of 43.2% for the case without additives and 8.6% for the case with additives. The reduction of extent of carbonation is due to increased pH from about 5 without additives to a value of 7.1 lowering dissolution of feedstock material. The same applies for a comparison with experimental data from Wang et al. [11]. With consideration of $1 mol_{NaHCO_3}/kg_{solvent}$ and $1 mol_{NaCl}/kg_{solvent}$ at $T = 185$ °C, $p = 34.5$ bar, and a simulation horizon of 5 h, the extent of carbonation is reduced to a value of 0.7 %, compared to a value of 66 % in the experimental study.

As the model does not account for surface enhancing effects of Na^+ on the dissolution of forsterite, the model cannot yet predict the beneficial influence of additives as shown experimentally. Still, we gain insight on shifts of solute concentrations resulting from consideration of additives in the system.

5. Conclusion and outlook

We propose a dynamic mechanistic model for direct mineral carbonation. We formulate general species mole balances that may be adapted to case studies of different minerals. The model accounts for interaction of multiple phases, i.e., gas, liquid, and three solid phases based on detailed thermodynamics and a population balance approach for solid phases. With simultaneous equilibrium and rate-based reactions, a reformulated DAE of differential index 1 is presented, and unknown parameter values and degrees of freedom are evaluated. We investigate the influence of contact angles of precipitating phases by comparison with experimental data from literature. We further use the model to simulate predictions for different model inputs. The simulations show qualitative agreement with experimental data while providing detailed information on, e.g., composition of the liquid phase and PSD. However, at the same time we show limits of the proposed model as the enhancing of additives is not yet represented correctly. Additionally, heterogeneous nucleation kinetics depending on shape and surface of dissimilar particles, i.e., contact angles between undissolved raw material particles and nucleating particles, need to be determined. To address these drawbacks, further research on influence of dissolved species and particle surface on kinetics of the solid-liquid interface is necessary. Furthermore, to evaluate heating, cooling, and potential usage of heat of reaction, the model needs to be extended for an energy balance. Moreover, alternative numerical schemes for the representation of PBE may be necessary depending on potential use of the model, e.g., optimization. We emphasize that this model is a first step to understand influences on mineral carbonation and point out that model extensions could lead to more precise results. Model extensions and different set-ups can be easily realized and alternative mineral carbonation systems can be investigated.

Declaration of Competing Interest

The authors declare that they have no known competing financial interests or personal relationships that could have appeared to influence the work reported in this paper.

Acknowledgements

This work was supported by the Federal Ministry of Education and Research (BMBF) in the CO2Min project (FKZ: 033RO14B), and by the German Research Foundation (DFG) under grant MI 1851/3-1.

Appendix A. Supplementary data

Supplementary data associated with this article can be found, in the online version, at https://doi.org/10.1016/j.cej.2020.126480.

References

[1] W. Seifritz, CO2 disposal by means of silicates, Nature 345 (6275) (1990) 486, https://doi.org/10.1038/345486b0.
[2] K.S. Lackner, Climate change. A guide to CO2 sequestration, Science 300 (5626) (2003) 1677–1678.https://doi.org/10.1126/science.1079033.
[3] R. Zevenhoven, J. Fagerlund, J.K. Songok, CO2 mineral sequestration: developments toward large-scale application, Greenh. Gases 1 (1) (2011) 48–57, https://doi.org/10.1002/ghg3.7.
[4] A. Sanna, M.R. Hall, M.M. Maroto-Valer, Post-processing pathways in carbon capture and storage by mineral carbonation (CCSM) towards the introduction of carbon neutral materials, Energy Environ. Sci. 5 (7) (2012) 7781, https://doi.org/10.1039/c2ee03455g.
[5] H. Zhao, Dadap N., A.-H.A. Park, Tailored synthesis of precipitated magensium carbonates as carbon-neutral filler materials during carbon mineral sequestration, Fluidization XIII: New Paradigm in Fluidization Engineering, Engineering Conferences International, New York, 2010.
[6] A. Sanna, M. Uibu, G. Caramanna, R. Kuusik, M.M. Maroto-Valer, A review of mineral carbonation technologies to sequester CO2, Chem. Soc. Rev. 43 (23) (2014) 8049–8080, https://doi.org/10.1039/c4cs00035h.
[7] A.A. Olajire, A review of mineral carbonation technology in sequestration of CO2, J. Pet. Sci. Eng. 109 (2013) 364–392, https://doi.org/10.1016/j.petrol.2013.03.013.
[8] W. O'Connor, D.C. Dahlin, Rush, S.J. Gerdemann, Aqueous Mineral Carbonation: Mineral Availability, Pretreatment, Reaction Parametrics, And Process Studies (2005).
[9] S.J. Gerdemann, W. O'Connor, D.C. Dahlin, L.R. Penner, H. Rush, Ex situ aqueous mineral carbonation, Environ. Sci. Technol. 41 (7) (2007) 2587–2593, https://doi.org/10.1021/es0619253.
[10] F. Wang, D. Dreisinger, M. Jarvis, T. Hitchins, D. Dyson, Quantifying kinetics of mineralization of carbon dioxide by olivine under moderate conditions, Chem. Eng. J. 360 (2019) 452–463, https://doi.org/10.1016/j.cej.2018.11.200.
[11] F. Wang, D. Dreisinger, M. Jarvis, T. Hitchins, Kinetics and mechanism of mineral carbonation of olivine for CO2 sequestration, Miner. Eng. 131 (2019) 185–197, https://doi.org/10.1016/j.mineng.2018.11.024.
[12] A.-H.A. Park, L.-S. Fan, CO2 mineral sequestration: physically activated dissolution of serpentine and pH swing process, Chem. Eng. Sci. 59 (22–23) (2004) 5241–5247, https://doi.org/10.1016/j.ces.2004.09.008.
[13] I.A. Munz, J. Kihle, O. Brandvoll, I. Machenbach, J.W. Carey, T.A. Haug, H. Johansen, N. Eldrup, A continuous process for manufacture of magnesite and silica from olivine, CO2 and H2O, Energy Proc. 1 (1) (2009) 4891–4898, https://doi.org/10.1016/j.egypro.2009.02.319.
[14] L.T. Biegler, Nonlinear programming: Concepts, algorithms, and applications to chemical processes, Society for Industrial and Applied Mathematics (SIAM 3600 Market Street Floor 6 Philadelphia PA 19104), Philadelphia, Pa., 2010. URL:

http://epubs.siam.org/ebooks/siam/mos-siam_series_on_optimization/mo10.
[15] A.M. Sahlodin, H.A.J. Watson, P.I. Barton, Nonsmooth model for dynamic simulation of phase changes, AIChE J. 62 (9) (2016) 3334–3351, https://doi.org/10.1002/aic.15378.
[16] T. Ploch, M. Glass, A.M. Bremen, R. Hannemann-Tamás, A. Mitsos, Modeling of dynamic systems with a variable number of phases in liquid-liquid equilibria, AIChE J. 65 (2) (2019) 571–581, https://doi.org/10.1002/aic.16447.
[17] W.R. Smith, R.W. Missen, Chemical Reaction Equilibrium Analysis: Theory and Algorithms, A Wiley-Interscience Publication, Wiley, New York, 1982.
[18] D.L. Parkhurst, C.A.J. Appelo, Description of input and examples for PHREEQC version 3-A computer program for speciation, batch-reaction, one-dimensional transport, and inverse geochemical calculations, Vol. 6 of Techniques and Methods, U.S. Geological Survey, 2013. URL: http://pubs.usgs.gov/tm/06/a43.
[19] D.A. Kulik, T. Wagner, S.V. Dmytrieva, G. Kosakowski, F.F. Hingerl, K.V. Chudnenko, U.R. Berner, GEM-Selektor geochemical modeling package: Revised algorithm and GEMS3K numerical kernel for coupled simulation codes, Comput. Geosci. 26 (012025) (2012) 189, https://doi.org/10.1007/s10596-012-9310-6.
[20] OLI Systems Inc., OLI Flowsheet: ESP (2020). URL: http://www.olisystems.com/.
[21] Aspen Technology Inc., Aspen Plus (2020). URL: https://www.aspentech.com/en/products/engineering/aspen-plus.
[22] Process Systems Enterprise Limited, gPROMS (2020). URL: https://www.psenterprise.com/products/gproms.
[23] J. Na, S. Park, J.H. Bak, M. Kim, D. Lee, Y. Yoo, I. Kim, J. Park, U. Lee, J.M. Lee, Bayesian inference of aqueous mineral carbonation kinetics for carbon capture and utilization, Ind. Eng. Chem. Res. 58 (19) (2019) 8246–8259, https://doi.org/10.1021/acs.iecr.9b01062.
[24] T.K. Oliver, F. Farhang, T.W. Hodgins, M.S. Rayson, G.F. Brent, T.S. Molloy, M. Stockenhuber, E.M. Kennedy, CO 2 capture modeling using heat-activated serpentinite slurries, Energy Fuels 33 (3) (2019) 1753–1766, https://doi.org/10.1021/acs.energyfuels.8b02823.
[25] W. Cheng, Z. Li, Controlled supersaturation precipitation of hydromagnesite for the MgCl2-NaCl system at elevated temperatures: chemical modeling and experiment, Ind. Eng. Chem. Res. 49 (4) (2010) 1964–1974, https://doi.org/10.1021/ie9015073.
[26] T.A. Haug, Dissolution and carbonation of mechanically activated olivine: Investigating CO2 sequestration possibilities, Dissertation, Norwegien University of Science and Technology, Trondheim, 2010.
[27] D. Daval, O. Sissmann, N. Menguy, G.D. Saldi, F. Guyot, I. Martinez, J. Corvisier, B. Garcia, I. Machouk, K.G. Knauss, R. Hellmann, Influence of amorphous silica layer formation on the dissolution rate of olivine at 90C and elevated pCO2, Chem. Geol. 284 (1) (2011) 193–209, https://doi.org/10.1016/j.chemgeo.2011.02.021.
[28] G. Gadikota, J. Matter, P. Kelemen, A.-H.A. Park, Chemical and morphological changes during olivine carbonation for CO2 storage in the presence of NaCl and NaCHO3, Phys. Chem. Chem. Phys. 16 (10) (2014) 4679–4693, https://doi.org/10.1039/C3CP54903H.
[29] F. Farhang, T.K. Oliver, M. Rayson, G.F. Brent, M. Stockenhuber, E. Kennedy, Experimental study on the precipitation of magnesite from thermally activated serpentine for CO2 sequestration, Chem. Eng. J. 303 (2016) 439–449, https://doi.org/10.1016/j.cej.2016.06.008.
[30] S.-Y. Pan, T.-C. Ling, A.-H.A. Park, P.-C. Chiang, An Overview: Reaction Mechanisms and Modelling of CO2 Utilization via Mineralization, Aerosol Air Qual. Res. 18 (4) (2018) 829–848, https://doi.org/10.4209/aaqr.2018.03.0093.
[31] D. Kremer, S. Etzold, J. Boldt, P. Blaum, K.M. Hahn, H. Wotruba, R. Telle, Geological mapping and characterization of possible primary input materials for the mineral sequestration of carbon dioxide in Europe, Minerals 9 (8) (2019) 485, https://doi.org/10.3390/min9080485.
[32] H. Ostovari, A. Sternberg, A. Bardow, Rock 'n' use of CO 2: carbon footprint of carbon capture and utilization by mineralization, Sustain. Energy Fuels 50 (5) (2020) 1004, https://doi.org/10.1039/d0se00190b.
[33] H.C. Helgeson, D.H. Kirkham, G.C. Flowers, Theoretical prediction of the thermodynamic behavior of aqueous electrolytes by high pressures and temperatures; IV, Calculation of activity coefficients, osmotic coefficients, and apparent molal and standard and relative partial molal properties to 600C and 5kb, Am. J. Sci. 281 (10) (1981) 1249–1516, https://doi.org/10.2475/ajs.281.10.1249.
[34] J.C. Tanger, H.C. Helgeson, Calculation of the thermodynamic and transport properties of aqueous species at high pressures and temperatures; revised equations of state for the standard partial molal properties of ions and electrolytes, Am. J. Sci. 288 (1) (1988) 19–98, https://doi.org/10.2475/ajs.288.1.19.
[35] J.W. Johnson, E.H. Oelkers, H.C. Helgeson, SUPCRT92: a software package for calculating the standard molal thermodynamic properties of minerals, gases, aqueous species, and reactions from 1 to 5000bar and 0 to 1000C, Comput. Geosci. 18 (7) (1992) 899–947, https://doi.org/10.1016/0098-3004(92)90029-Q.
[36] W. Wagner, H.-J. Kretzschmar (Eds.), International Steam Tables, Springer, Berlin Heidelberg, Berlin, Heidelberg, 2008, , https://doi.org/10.1007/978-3-540-74234-0.
[37] D.-Y. Peng, D.B. Robinson, A new two-constant equation of state, Ind. Eng. Chem. Fund. 15 (1) (1976) 59–64, https://doi.org/10.1021/i160057a011.
[38] A. Mersmann, Crystallization Technology Handbook, Dekker, New York, NY, 1995.
[39] A.C. Lasaga, Chapter 2. Fundamental approaches in describing mineral dissolution and precipitation rates, in: A.F. White, S.L. Brantley, A.F. White, S.L. Brantley (Eds.), Chemical Weathering Rates of Silicate Minerals, De Gruyter, Berlin, Boston, 1995, pp. 23–86, , https://doi.org/10.1515/9781501509650-004.
[40] K. Zimmer, Y. Zhang, P. Lu, Y. Chen, G. Zhang, M. Dalkilic, C. Zhu, SUPCRTBL: a revised and extended thermodynamic dataset and software package of SUPCRT92, Comput. Geosci. 90 (2016) 97–111, https://doi.org/10.1016/j.cageo.2016.02.013.
[41] L.A. Bromley, Thermodynamic properties of strong electrolytes in aqueous solutions, AIChE J. 19 (2) (1973) 313–320, https://doi.org/10.1002/aic.690190216.
[42] H.P. Meissner, Prediction of activity coefficients of strong electrolytes in aqueous systems, in: S.A. Newman, H.E. Barner, M. Klein, S.I. Sandler (Eds.), Thermodynamics of Aqueous Systems with Industrial Applications, Vol. 133 of ACS Symposium Series, American Chemical Society, Washington D.C., 1980, pp. 495–511, , https://doi.org/10.1021/bk-1980-0133.ch025.
[43] J.L. Palandri, Y.K. Kharaka, A compilation of rate parameters of water-mineral interaction kinetics for application to geochemical modeling, Open File Report 2004–1068, US Geological Survey, Menlo Park, CA, 2004.
[44] I. Søreide, C.H. Whitson, Peng-Robinson predictions for hydrocarbons, CO2, N2, and H2S with pure water and NaCl brine, Fluid Phase Equilib. 77 (1992) 217–240, https://doi.org/10.1016/0378-3812(92)85105-H.
[45] J.J. Rosso, J.D. Rimstidt, A high resolution study of forsterite dissolution rates, Geochim. Cosmochim. Acta 64 (5) (2000) 797–811, https://doi.org/10.1016/S0016-7037(99)00354-3.
[46] M. Hänchen, S. Krevor, M. Mazzotti, K.S. Lackner, Validation of a population balance model for olivine dissolution, Chem. Eng. Sci. 62 (22) (2007) 6412–6422, https://doi.org/10.1016/j.ces.2007.07.065.
[47] M. Hänchen, V. Prigiobbe, R. Baciocchi, M. Mazzotti, Precipitation in the Mg-carbonate system-effects of temperature and CO2 pressure, Chem. Eng. Sci. 63 (4) (2008) 1012–1028, https://doi.org/10.1016/j.ces.2007.09.052.
[48] T. Allers, Instationäre Partikelauflösung und Kristallisation in dreiphasigen Reaktionsprozessen, Fortschritt-Berichte VDI Reihe 3 vol. 681, VDI-Verlag, Düsseldorf, Verfahrenstechnik, 2001.
[49] N.V. Mantzaris, P. Daoutidis, F. Srienc, Numerical solution of multi-variable cell population balance models. III. Finite element methods, Comput. Chem. Eng. 25 (11–12) (2001) 1463–1481, https://doi.org/10.1016/S0098-1354(01)00711-6.
[50] N.V. Mantzaris, P. Daoutidis, F. Srienc, Numerical solution of multi-variable cell population balance models. II. Spectral methods, Comput. Chem. Eng. 25 (11–12) (2001) 1441–1462, https://doi.org/10.1016/S0098-1354(01)00710-4.
[51] N.V. Mantzaris, P. Daoutidis, F. Srienc, Numerical solution of multi-variable cell population balance models: I. Finite difference methods, Comput. Chem. Eng. 25 (11–12) (2001) 1411–1440, https://doi.org/10.1016/S0098-1354(01)00709-8.
[52] H. Muhr, R. David, J. Villermaux, P. Jezequel, Crystallization and precipitation engineering-VI. Solving population balance in the case of the precipitation of silver bromide crystals with high primary nucleation rates by using the first order upwind differentiation, Chem. Eng. Sci. 51 (2) (1996) 309–319, https://doi.org/10.1016/0009-2509(95)00257-X.
[53] S. Kumar, D. Ramkrishna, On the solution of population balance equations by discretization – III. Nucleation, growth and aggregation of particles, Chem. Eng. Sci. 52 (24) (1997) 4659–4679, https://doi.org/10.1016/S0009-2509(97)00307-2.
[54] T.J.B. Holland, R. Powell, An improved and extended internally consistent thermodynamic dataset for phases of petrological interest, involving a new equation of state for solids, J. Metamorph. Geol. 29 (3) (2011) 333–383, https://doi.org/10.1111/j.1525-1314.2010.00923.x.
[55] L. Haar, J.S. Gallagher, G.S. Kell, NBS/NRC Steam Tables: Thermodynamic and Transport Properties and Computer Programs for Vapor and Liquid States of Water in SI Units, Taylor & Francis, Bristol, Pa, 1984.
[56] G.D. Miron, A.M.M. Leal, A. Yapparova, Thermodynamic properties of aqueous species calculated using the HKF model: how do different thermodynamic and electrostatic models for solvent water affect calculated aqueous properties? Geofluids 2019 (a43) (2019) 1–24, https://doi.org/10.1155/2019/5750390.
[57] K.E. Brenan, S.L. Campbell, L.R. Petzold, Numerical solution of initial-value problems in differential-algebraic equations, Soc. Ind. Appl. Math. (1995), https://doi.org/10.1137/1.9781611971224.
[58] H.I. Moe, S. Hauan, K.M. Lien, T. Hertzberg, Dynamic model of a system with phase- and reaction equilibrium, Comput. Chem. Eng. 19 (1995) 513–518, https://doi.org/10.1016/0098-1354(95)87088-1.
[59] A. Kumar, P.D. Christofides, P. Daoutidis, Singular perturbation modeling of nonlinear processes with nonexplicit time-scale multiplicity, Chem. Eng. Sci. 53 (8) (1998) 1491–1504, https://doi.org/10.1016/S0009-2509(98)00006-2.
[60] N. Vora, P. Daoutidis, Nonlinear model reduction of chemical reaction systems, AIChE J. 47 (10) (2001) 2320–2332, https://doi.org/10.1002/aic.690471016.
[61] P. Daoutidis, DAEs in model reduction of chemical processes: an overview, in: A. Ilchmann, T. Reis (Eds.), Surveys in Differential-Algebraic Equations II, Springer International Publishing, Cham, 2015, pp. 69–102 URL: https://link.springer.com/chapter/10.1007/978-3-319-11050-9_2.
[62] O. Walz, C. Marks, J. Viell, A. Mitsos, Systematic approach for modeling reaction networks involving equilibrium and kinetically-limited reaction steps, Comput. Chem. Eng. 98 (2017) 143–153, https://doi.org/10.1016/j.compchemeng.2016.12.014.
[63] A.I. Kakhu, C.C. Pantelides, Dynamic modelling of aqueous electrolyte systems, Comput. Chem. Eng. 27 (6) (2003) 869–882, https://doi.org/10.1016/S0098-1354(03)00002-4.
[64] A. Zinser, L. Rihko-Struckmann, K. Sundmacher, Dynamic method for computation of chemical and phase equilibria, Comput. Chem. Eng. 89 (2016) 1–10, https://doi.org/10.1016/j.compchemeng.2016.02.014.
[65] H. Guo, Y. Huang, Y. Chen, Q. Zhou, Quantitative Raman Spectroscopic Measurements of CO2 Solubility in NaCl Solution from (273.15 to 473.15) K at p = (10.0, 20.0, 30.0, and 40.0) MPa, J. Chem. Eng. Data 61(1) (2015) 466–474. https://doi.org/10.1021/acs.jced.5b00651.
[66] N. Spycher, K. Pruess, A phase-partitioning model for CO2-brine mixtures at elevated temperatures and pressures: application to CO2-enhanced geothermal systems, Transp. Porous Media 82 (1) (2010) 173–196, https://doi.org/10.1007/s11242-009-9425-y.

[67] X. Li, C. Peng, J.P. Crawshaw, G.C. Maitland, J.M. Trusler, The pH of CO2-saturated aqueous NaCl and NaCHO3 solutions at temperatures between 308K and 373K at pressures up to 15MPa, Fluid Phase Equilib. 458 (2018) 253–263, https://doi.org/10.1016/j.fluid.2017.11.023.
[68] Modelica (2020). URL: https://www.modelica.org/.
[69] Dassault Systëmes AB, Dymola: Dynamic Modeling Laboratory (2020). URL: https://www.3ds.com/products-services/catia/products/dymola/.
[70] L.R. Petzold, A Description of DASSL: A Differential/Algebraic System Solver, SAND82-8637, Sandia National Laboratories (1982).
[71] Q.R.S. Miller, H.T. Schaef, J.P. Kaszuba, G. Gadikota, B.P. McGrail, K.M. Rosso, Quantitative review of olivine carbonation kinetics: reactivity trends, mechanistic insights, and research frontiers, Environ. Sci. Technol. Lett. 6 (8) (2019) 431–442, https://doi.org/10.1021/acs.estlett.9b00301.
[72] H. Bearat, M.J. McKelvy, A.V.G. Chizmeshya, D. Gormley, R. Nunez, R.W. Carpenter, K. Squires, G.H. Wolf, Carbon sequestration via aqueous olivine mineral carbonation: role of passivating layer formation, Environ. Sci. Technol. 40 (15) (2006) 4802–4808, https://doi.org/10.1021/es0523340.
[73] S. Stopic, C. Dertmann, I. Koiwa, D. Kremer, H. Wotruba, S. Etzold, R. Telle, P. Knops, B. Friedrich, Synthesis of nanosilica via olivine mineral carbonation under high pressure in an autoclave, Metals 9 (6) (2019) 708, https://doi.org/10.3390/met9060708.
[74] A.V.G. Chizmeshya, M.J. McKelvy, K. Squires, R.W. Carpenter, H. Bëarat, A Novel Approach to Mineral Carbonation: Enhancing Carbonation while Avoiding Mineral Pretreatment Process Cost, Final Report 9224162, U.S. Department of Energy, Washington, DC, 2007.
[75] A.-H.A. Park, R. Jadhav, L.-S. Fan, CO2 mineral sequestration: chemically enhanced aqueous carbonation of serpentine, Can. J. Chem. Eng. 81 (3–4) (2003) 885–890, https://doi.org/10.1002/cjce.5450810373.
[76] D. Weidener, H. Klose, W. Leitner, U. Schurr, B. Usadel, P. Domínguez de María, P.M. Grande, One-step lignocellulose fractionation by using 2,5-furandicarboxylic acid as a biogenic and recyclable catalyst, ChemSusChem 11 (13) (2018) 2051–2056, https://doi.org/10.1002/cssc.201800653.